PHYSICAL REVIEW D **90,** 054027 (2014)

NLO supersymmetric-QCD corrections to stop pair associated by Z^0 production at the LHC

Hisham A. El-Kolaly*

Faculty of Science, Physics Department, Cairo University, Giza 12613, Egypt

(Received 25 November 2013; published 26 September 2014)

We present the calculations of the production of $\tilde{t}_1\,\bar{\tilde{t}}_1\,Z^0$ in the minimal supersymmetric standard model at the Large Hadron Collider at center-of-mass energies of 7 and 14 TeV. We discuss the impact of the next-to-leading-order supersymmetric-QCD corrections on the cross sections of $\tilde{t}_1\,\bar{\tilde{t}}_1\,Z^0$ production and on the transverse-momentum distributions of the final stop quark. The uncertainties of the leading-order and supersymmetric-QCD corrected cross sections due to the renormalization/factorization scale are studied. Calculations demonstrate that the next-to-leading-order supersymmetric-QCD corrections improve the scale dependence of the leading-order cross sections and enhance significantly the transverse-momentum distributions.

DOI: 10.1103/PhysRevD.90.054027 PACS numbers: 13.85.-t, 14.80.Da

I. INTRODUCTION

Supersymmetry (SUSY) provides a particularly interesting subject for studies of the detailed analysis of physics beyond the standard model (SM) [1]. If SUSY does give a correct model of nature, the proton-proton collider LHC will be expected to determine the SUSY parameters. The simplest supersymmetric model [the minimal supersymmetric extension of the standard model (MSSM)] [2,3] is a generalization of the SM theory with a minimal number of introduced SUSY partners. Supersymmetry predicts the existence of scalar partners $\tilde{f}_L, \tilde{f}_R$ to each SM chiral fermion, which mix to produce two mass eigenstates $\tilde{f}_1$ and $\tilde{f}_2$ and spin-1/2 partners to the gauge bosons and to the scalar Higgs bosons. Unfortunately, MSSM has many parameters, undetermined by the moment, and different choices for these parameters yield qualitatively different realizations of possible new physics. Thus, the phenomenology of SUSY is quite complex. As a result, most of the analyses of the direct search results are carried out by invoking additional theoretical assumptions, which restricts the number of parameters. In particular, the minimal supersymmetric gravity model (mSUGRA) [4] has been used most extensively. In mSUGRA, it is assumed that the left- and right-handed squarks ($\tilde{q_L}$ and $\tilde{q_R}$), the left- and right-handed sleptons ($\tilde{l_L}$ and $\tilde{l_R}$), and the Higgs bosons have a common soft-breaking mass (m_0) at the grand unified theory scale (M_G). Moreover, the gaugino masses and the trilinear soft-breaking terms are also assigned common values $m_{1/2}$ and A_0, respectively, at M_G. The number of free parameters is further reduced by requiring radiative $SU(2) \times U(1)$ breaking at the electroweak scale [5]. This fixes the magnitude of the Higgsino mass parameter (μ). Thus, m_0, $m_{1/2}$, and A_0 along with the sign of μ and $\tan\beta$ (the ratio of the vacuum expectation values of the two neutral Higgs bosons) define the model completely.

SUSY must be broken in the practical world, and the sparticle mass spectrum depends on the SUSY-breaking mechanism. The fundamental MSSM parameters need to be determined from the precise measurement of the masses, production cross sections, and decay widths of these superpartners. With these parameters, we can reconstruct the SUSY-breaking mechanism and probe the MSSM.

At hadron colliders, QCD effects are particularly important and must be taken into account to obtain precise theoretical predictions. Since at high energies QCD is a perturbative quantum field theory, QCD effects at collider energies can be calculated order by order in the strong coupling constant. The lowest order at which a process can be calculated, the leading order (LO), typically has a large theoretical uncertainty associated with it. This is mainly due to the opening of new production channels at higher orders of the perturbative series and to the large dependence of LO calculations on renormalization and factorization scales, in certain renormalization prescriptions. Adding the first-order QCD corrections, that is, next-to-leading-order (NLO) corrections, usually improves the stability of theoretical predictions considerably and tests the behavior of the perturbative expansion.

The associated production of a weak gauge boson with two light stops constitutes not only an important background process to Higgs boson searches for light Higgs bosons ($M_h < 135$ GeV) and many searches for signals of new physics but also represents a unique opportunity to test and improve the theoretical prediction for stop at hadron colliders. This last task becomes essential when the signal to background ratio is small and the background cannot be easily extracted from data. Typically, this is the case for processes that involve a large number of kinematic variables and that have broad kinematic distributions, as often arises when final states consist of several particles.

*kolaly@sci.cu.edu.eg

In Ref. [6], we presented detailed calculations of the NLO SUSY-QCD cross section corrections to the production of a lightest stop pair in association with the MSSM Higgs boson at the 14 TeV LHC. It was found that the renormalization/factorization scale dependence of the lowest-order total cross section is strong. Including the NLO SUSY-QCD corrections significantly reduces and stabilizes the dependence of the lowest-order total cross section on the renormalization/factorization scale.

In this paper, we present the calculation of NLO SUSY-QCD corrections to the production of a Z^0 weak gauge boson in association with a top-antitop squark pair at hadron colliders ($pp \to \tilde{t}_1 \bar{\tilde{t}}_1 Z^0$) at the 7 and 14 TeV LHC and studied their uncertainties induced by the factorization/renormalization scale. In Sec. II, we present the tree-level calculations for the cross sections of the process $pp \to \tilde{t}_1 \bar{\tilde{t}}_1 Z^0$ at the 7 and 14 TeV LHC. In Sec. III, we provide a description of the calculation of the NLO SUSY-QCD corrections. Numerical results for the total cross sections and transverse-momentum distributions at the LHC are presented in Sec. IV. Finally, the conclusion is given in Sec. V.

II. LO PROCESSES AND CONVENTIONS

In the MSSM Lagrangian, mixing of the left- and right-handed top-squark eigenstates $\tilde{t}_{L/R}$ into mass eigenstates $\tilde{t}_{1/2}$ is induced by the trilinear Higgs-stop-stop coupling term A_t and the Higgs-mixing parameter μ. The top-squark mass matrix squared is given by [7]

$$\mathbf{M}^2 = \begin{pmatrix} m_t^2 + A_{LL} & m_t B_{LR} \\ m_t B_{LR} & m_t^2 + C_{RR} \end{pmatrix}, \tag{1}$$

with m_t denoting the top-quark mass and

$$\begin{aligned} A_{LL} &= \left(\frac{1}{2} - \frac{2}{3}\sin^2\theta_W\right) m_Z^2 \cos 2\beta + m_{\tilde{Q}_3}^2, \\ B_{LR} &= A_t - \mu \cot\beta, \\ C_{RR} &= \frac{2}{3}\sin^2\theta_W m_Z^2 \cos 2\beta + m_{\tilde{U}_3}^2. \end{aligned} \tag{2}$$

Here, $m_{\tilde{Q}_3}, m_{\tilde{U}_3}$ are the soft-breaking mass terms for left- and right-handed top squarks, respectively.

The top-squark mass eigenvalues are obtained by diagonalizing the mass matrix

$$U\mathbf{M}^2U^\dagger = \begin{pmatrix} m_{\tilde{t}_1}^2 & 0 \\ 0 & m_{\tilde{t}_2}^2 \end{pmatrix}, \qquad U = \begin{pmatrix} \cos\theta_{\tilde{t}} & \sin\theta_{\tilde{t}} \\ -\sin\theta_{\tilde{t}} & \cos\theta_{\tilde{t}} \end{pmatrix}, \tag{3}$$

$$m_{\tilde{t}_{1,2}}^2 = m_t^2 + \frac{1}{2}\Big(A_{LL} + C_{RR} \mp \sqrt{(A_{LL} - C_{RR})^2 + 4m_t^2 B_{LR}^2}\Big), \tag{4}$$

and the mixing angle $\theta_{\tilde{t}}$ is determined by

$$\tan 2\theta_{\tilde{t}} = \frac{2m_t B_{LR}}{A_{LL} - C_{RR}}. \tag{5}$$

The production of the Z^0 boson in association with a pair of top squarks proceeds at LO through the partonic processes

$$q(p_1) + \bar{q}(p_2) \to \tilde{t}_1(p_3) + \bar{\tilde{t}}_1(p_4) + Z^0(p_5) \quad (q = u, d)$$

and

$$g(p_1) + g(p_2) \to \tilde{t}_1(p_3) + \bar{\tilde{t}}_1(p_4) + Z^0(p_5), \tag{6}$$

where we denote the external four-momenta by p_i $(i = 1, \ldots, 5)$. The corresponding generic Feynman diagrams that contribute to the LO processes (6) are displayed in Fig. 1.

The lowest-order cross sections for the subprocesses $q\bar{q}, gg \to \tilde{t}_1 \bar{\tilde{t}}_1 Z$ are obtained by using the following formula:

$$\begin{aligned} d\hat{\sigma}_{q\bar{q}}^{\mathrm{LO}} &= \frac{1}{36}\frac{(2\pi)^4}{2\hat{s}} \sum_{\mathrm{spin}}^{\mathrm{color}} |\mathcal{M}_{\mathrm{LO}}^{q\bar{q}}|^2 d\Omega_3, \\ d\hat{\sigma}_{gg}^{\mathrm{LO}} &= \frac{1}{256}\frac{(2\pi)^4}{2\hat{s}} \sum_{\mathrm{spin}}^{\mathrm{color}} |\mathcal{M}_{\mathrm{LO}}^{gg}|^2 d\Omega_3, \end{aligned} \tag{7}$$

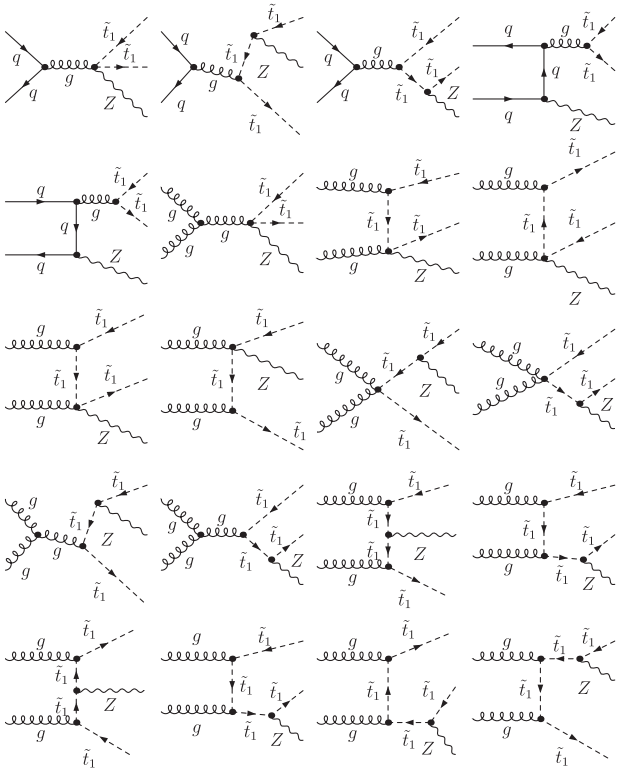

FIG. 1. The LO Feynman diagrams for the $q\bar{q} \to \tilde{t}_1 \bar{\tilde{t}}_1 Z^0$ and $gg \to \tilde{t}_1 \bar{\tilde{t}}_1 Z^0$ subprocesses.

where the factors $\frac{1}{36}$, and factors $\frac{1}{256}$ in Eqs. (7), result from the average over the initial-state spins and colors of the initial partons, $\hat{s}$ is the partonic center-of-mass energy squared, and $\mathcal{M}_{\rm LO}^{q\bar{q}}$ and $\mathcal{M}_{\rm LO}^{gg}$ are the amplitudes of all the tree-level diagrams for the partonic processes $q\bar{q} \to \tilde{t}_1 \bar{\tilde{t}}_1 Z^0$ and $gg \to \tilde{t}_1 \bar{\tilde{t}}_1 Z^0$, respectively. The phase-space elements $d\Omega_3$ in Eqs. (7) are expressed as

$$d\Omega_3 = \delta^{(4)}\left(p_1 + p_2 - \sum_{i=3}^{5} p_i\right) \prod_{j=3}^{5} \frac{d^3\boldsymbol{p}_j}{(2\pi)^3 2E_j}. \quad (8)$$

The LO total cross section of $pp \to \tilde{t}_1 \bar{\tilde{t}}_1 Z$ can be expressed as

$$\sigma^{\rm LO} = \sum_{ij=q\bar{q},gg} \int_0^1 dx_1 \int_0^1 dx_2 [\mathcal{F}_i^P(x_1,\mu)\mathcal{F}_j^P(x_2,\mu) + (1 \leftrightarrow 2)]\hat{\sigma}_{ij}^0(\hat{s}), \quad (9)$$

where $\mathcal{F}_i^P(x_1,\mu)$ are the parton distribution functions (PDFs) with parton i in a proton, The partonic colliding energy squared $\hat{s} = x_1 x_2 s$, where s is defined as the center-of-mass energy squared of the proton-(anti)proton collision. μ is the factorization energy scale.

III. NLO SUSY-QCD CORRECTIONS

The NLO SUSY-QCD corrections consist of both virtual corrections to the tree-level processes and one-parton real radiation from both the initial and final states. The NLO SUSY-QCD partonic cross section reads

$$\hat{\sigma}_{ij}^{\rm NLO} = \hat{\sigma}_{ij}^{\rm LO} + \delta\hat{\sigma}_{ij}^{\rm NLO}, \quad (10)$$

where $\hat{\sigma}_{ij}^{\rm LO}$ denotes the LO partonic cross section and $\delta\hat{\sigma}_{ij}^{\rm NLO}$ describes the corrections to $\hat{\sigma}_{ij}^{\rm LO}$. The NLO corrections $\delta\hat{\sigma}_{ij}^{\rm NLO}$ receive contributions from $q\bar{q}$, gg, qg, and $\bar{q}g$ initiated processes and can be decomposed in the following way:

$$\delta\hat{\sigma}_{ij}^{\rm NLO} = \int d(PS_3)\overline{\sum}|\mathcal{M}_{\rm virt}|^2 + \int d(PS_4)\overline{\sum}|\mathcal{M}_{\rm real}|^2 \equiv \hat{\sigma}_{ij}^{\rm virt} + \hat{\sigma}_{ij}^{\rm real}, \quad (11)$$

where the term integrated over the phase-space measure $d(PS_3)$ corresponds to the virtual one-loop corrections with three particles in the final state, while the one integrated over the phase-space measure $d(PS_4)$ corresponds to the real tree-level corrections with one additional emitted parton. The sum $\overline{\sum}$ indicates that the corresponding amplitudes squared $|\mathcal{A}_{\rm virt(real)}|^2$ have been averaged over the initial-state degrees of freedom and summed over the final-state ones.

A. Virtual corrections

The virtual corrections consist of the one-loop corrections to the LO reactions. One can classify the corrections into self-energy corrections, vertex corrections, box-type corrections, and pentagon-type corrections where all the external legs are connected to one loop, thus forming a pentagon. Feynman diagrams and amplitudes have been generated with the FeynArts package [8]. For demonstration, some pentagon diagrams are illustrated in Figs. 2 and 3 to $q\bar{q} \to \tilde{t}_1 \bar{\tilde{t}}_1 Z^0$ and $gg \to \tilde{t}_1 \bar{\tilde{t}}_1 Z^0$ processes, respectively. The calculation of the virtual diagrams has been performed using dimensional regularization, always in $d = 4 - 2\epsilon$ dimensions, and adopts the modified minimal subtraction ($\overline{\rm MS}$) scheme to renormalize the strong coupling constant and the relevant masses and fields, except for top squark and gluon, where their masses and wave functions are renormalized by applying the on-shell scheme. The diagrams have been evaluated using FORM [9] and Mathematica, and all tensor integrals have been reduced to linear combinations of a fundamental set of scalar one-loop integrals using standard techniques [10]. The scalar integrals which give rise to either ultraviolet (UV) or infrared (IR) singularities have been computed analytically, while finite scalar integrals have been evaluated using standard packages [11].

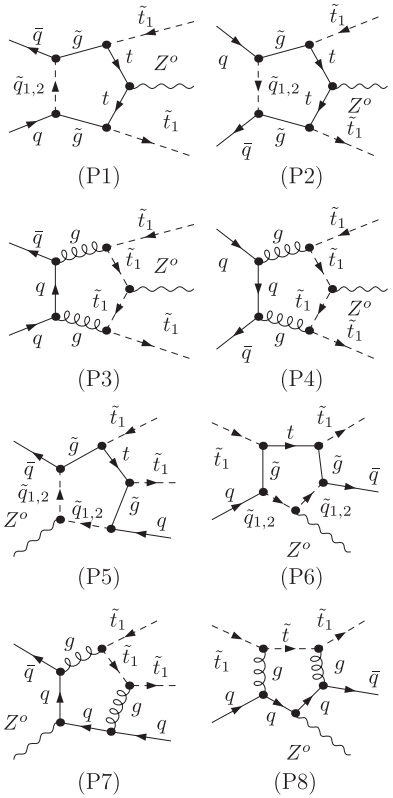

FIG. 2. A generic set of SUSY-QCD pentagon diagrams in the subprocesses $q\bar{q} \to \tilde{t}_1 \bar{\tilde{t}}_1 Z^0$.

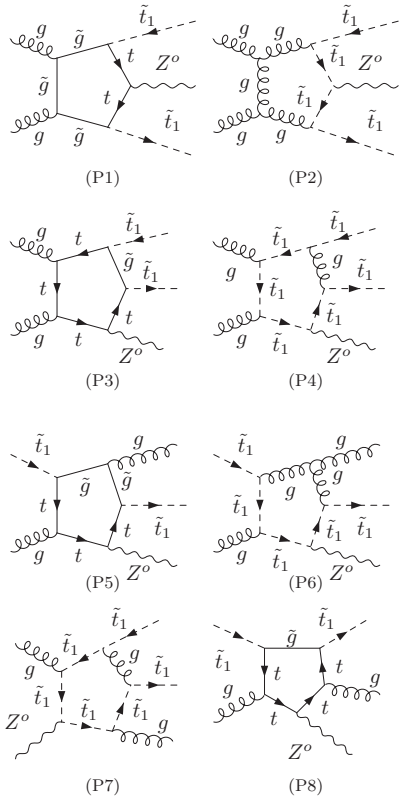

FIG. 3. A generic set of SUSY-QCD pentagon diagrams in the subprocesses $gg \to \tilde{t}_1 \bar{\tilde{t}}_1 Z^0$.

Box and pentagon diagrams are ultraviolet finite but have infrared singularities. The calculations of many of the box scalar integrals and, in particular, of the pentagon scalar integrals are the most complicated ones, due to the large number of massive particles present in the final state and in the loop. The five-point scalar integrals are reduced to a sum of five scalar four-point functions, plus terms of $O(\epsilon)$ which can be neglected [12–14].

Self-energy and vertex diagrams contain both IR and UV divergences. The UV divergences are renormalized by introducing a suitable set of counterterms. Since the cross section is a renormalization group invariant, the total NLO SUSY-QCD amplitudes of partonic processes $q\bar{q} \to \tilde{t}_1 \bar{\tilde{t}}_1 Z^0$ and $gg \to \tilde{t}_1 \bar{\tilde{t}}_1 Z^0$ are UV finite after we renormalize the wave function of the external fields, the top-squark mass, and the coupling constants. We perform the renormalization program in the on-shell scheme where the quark and squark masses are defined as the poles of their respective propagators. The renormalization of the strong gauge coupling constant g_s is carried out in the $\overline{\text{MS}}$ renormalization scheme.

The Feynman rules for the counterterms can be expressed in terms of the field renormalization constants of quarks, squarks, and gluons. We express the bare quantities by the renormalized ones

$$\Psi_{q_a}^{\text{bare}} = \Psi_{q_a}^{\text{ren}}\left(1+\frac{1}{2}\delta Z_a^q\right),$$
$$\Phi_{\tilde{q}_i}^{\text{bare}} = \Phi_{\tilde{q}_i}^{\text{ren}}\left(1+\frac{1}{2}\delta Z_{\tilde{t}_i}\right),$$
$$G_\mu^{\text{bare}} = G_\mu^{\text{ren}}\left(1+\frac{1}{2}\delta Z_G\right), \tag{12}$$

together with the renormalization constants for the strong coupling, for the strong Yukawa coupling, and for the squark masses, which are defined according to

$$g_s^{\text{bare}} = g_s^{\text{ren}}(1+\delta Z_g),$$
$$\hat{g}_s^{\text{bare}} = \hat{g}_s^{\text{ren}}(1+\delta Z_{\tilde{g}}),$$
$$m_{\tilde{q}_i}^{2\text{bare}} = m_{\tilde{q}_i}^{2\text{ren}} + \delta m_{\tilde{q}_i}^2. \tag{13}$$

The renormalized quark self-energies $\hat{\Sigma}^q(p^2)$ are obtained from the unrenormalized quark self-energies $\Sigma^q(p^2)$ according to

$$\hat{\Sigma}^q(p^2) = \Sigma^q(p^2) + \not{p}\omega_- \delta Z_L^q + \not{p}\omega_+ \delta Z_R^q - \frac{m_q}{2}\delta Z_L^q + \delta Z_R^q + \delta m_q. \tag{14}$$

The renormalization constants of the quarks are obtained via on-shell conditions [15] as follows:

$$\delta Z_a^q = -\text{Re}\{\Sigma_a^q(m_q^2)\} - m_q^2 \text{Re}\left\{\frac{\partial}{\partial p^2}(\Sigma_L^q(p^2) + \Sigma_R^q(p^2) + 2\Sigma_S^q(p^2))\right\}_{p^2=m_q^2} \quad (a = L, R). \tag{15}$$

The renormalized self-energies of squarks $\hat{\Sigma}_{\tilde{q}_i}$ (for $i = 1, 2$) are obtained from the unrenormalized self-energies according to [16,17]

$$\hat{\Sigma}_{\tilde{q}_i}(p^2) = \Sigma_{\tilde{q}_i}(p^2) + p^2 \delta Z_{\tilde{q}_i} - m_{\tilde{q}_i}^2 \delta Z_{\tilde{q}_i} - \delta m_{\tilde{q}_i}^2, \tag{16}$$

where renormalization constants of the top squark are determined by the on-shell conditions

$$\delta Z_{\tilde{q}_i} = -\text{Re}\left\{\frac{\partial \Sigma_{\tilde{q}_i}(p^2)}{\partial p^2}\right\}_{|p^2=m_{\tilde{q}_i}^2}, \tag{17}$$

$$\delta m_{\tilde{q}_i}^2 = \text{Re}\{\Sigma_{\tilde{q}_i}(m_{\tilde{q}_i}^2)\}. \tag{18}$$

The full set of virtual contributions is UV finite after including the proper counterterms for self-energies, squark triple and quartic vertices, and quark vertices, as listed in the following set of Feynman rules [6,18]:

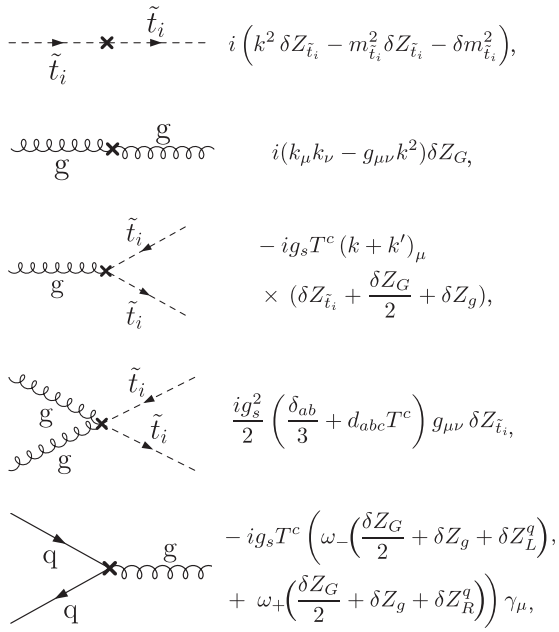

where k, k' denote the momenta of top squarks (in the direction of arrows), a, b, and c are the gluonic color indices, T^c and d_{abc} are the color factors (we skip the fermionic and sfermionic color indices), and $\omega_\pm = (1 \pm \gamma_5)/2$ are the projection operators.

The renormalized amplitudes of all the NLO SUSY-QCD virtual corrections to the partonic processes $q\bar{q} \to \tilde{t}_1\,\bar{\tilde{t}}_1\,Z^0$ and $gg \to \tilde{t}_1\,\bar{\tilde{t}}_1\,Z^0$ in the MSSM are expressed as

$$\delta\mathcal{M}_{ij}^{\rm virt} = \delta\mathcal{M}_{ij}^{\rm self} + \delta\mathcal{M}_{ij}^{\rm tri} + \delta\mathcal{M}_{ij}^{\rm box} + \delta\mathcal{M}_{ij}^{\rm pent} + \delta\mathcal{M}_{ij}^{\rm count} \quad (ij = u\bar{u}, d\bar{d}, gg), \tag{19}$$

where $\delta\mathcal{M}_{ij}^{\rm self}$, $\delta\mathcal{M}_{ij}^{\rm tri}$, $\delta\mathcal{M}_{ij}^{\rm box}$, $\delta\mathcal{M}_{ij}^{\rm pent}$, and $\delta\mathcal{M}_{ij}^{\rm count}$ represent the amplitudes for self-energy, triangle, box, pentagon, and counterterm diagrams, respectively. Then, we can get the UV-finite virtual NLO QCD correction component $\hat{\sigma}_{ij}^{\rm virt}$ as

$$\hat{\sigma}_{ij}^{\rm virt} = \frac{1}{2|\vec{p}_1|\sqrt{\hat{s}}}\int {\rm d}\Gamma_3 \overline{\sum}{\rm Re}(\mathcal{M}_{ij}^{\rm LO} \times \delta\mathcal{M}_{ij}^{\rm virt}). \tag{20}$$

B. Real corrections

The NLO real cross section corrections $\delta\hat{\sigma}_{gg}^{\rm real}$ and $\delta\hat{\sigma}_{q\bar{q}}^{\rm real}$ due to the emission of a real gluon, i.e., to the processes $q\bar{q}(gg) \to \tilde{t}_1\,\bar{\tilde{t}}_1\,Z^0 g$, contain IR singularities. These singularities can be either *soft*, when the energy of the emitted gluon becomes very small, or *collinear*, when the final-state gluon is emitted collinear to one of the initial partons. There is no collinear radiation from the final $\tilde{t}_1$ and $\bar{\tilde{t}}_1$ quarks because they are massive. At the same order in α_s, the $\delta\hat{\sigma}_{qg}^{\rm real}$ cross section corresponds to the tree-level processes $(q,\bar{q})g \to \tilde{t}_1\,\bar{\tilde{t}}_1\,Z^0(q,\bar{q})$ and develops IR singularities due to the collinear emission of a final-state quark or antiquark from one of the initial-state massless partons.

The IR singularities can be conveniently isolated by *slicing* the $(q\bar{q})gg \to \tilde{t}_1\,\bar{\tilde{t}}_1\,Z^0 g$ and $(q,\bar{q})g \to \tilde{t}_1\,\bar{\tilde{t}}_1\,Z^0(q,\bar{q})$ phase spaces into different regions defined by suitable cutoffs. We use the two-cutoff phase-space slicing method to perform the integration over the phase space of these real emission processes [19–21]. In our calculations, the real gluon emission correction to each of the processes $(q\bar{q})gg \to \tilde{t}_1\,\bar{\tilde{t}}_1\,Z^0$ contains both soft and collinear IR singularities, which are involved in the soft gluon region ($E_6 \le \delta_s\sqrt{\hat{s}}/2$) and the hard gluon region ($E_6 > \delta_s\sqrt{\hat{s}}/2$), respectively. The hard gluon region is also divided into the hard-collinear region (HC) and the hard-noncollinear region ($\overline{\rm HC}$) with $\frac{2p_i\cdot p_6}{E_6\sqrt{\hat{s}}} < \delta_c$ and $\frac{2p_i\cdot p_6}{E_6\sqrt{\hat{s}}} \ge \delta_c$ (p_i are the momenta for q and $\bar{q}$):

$$\hat{\sigma}_{g,ij}^{\rm real}(ij \to t\bar{t}\gamma g) = \hat{\sigma}_{g,ij}^{\rm soft} + \hat{\sigma}_{g,ij}^{\rm hard} \quad (ij = q\bar{q}, gg),$$
$$\hat{\sigma}_{g,ij}^{\rm hard}(ij \to t\bar{t}\gamma g) = \hat{\sigma}_{g,ij}^{\rm HC} + \hat{\sigma}_{g,ij}^{\overline{\rm HC}}. \tag{21}$$

Each of the real light-(anti)quark emission processes contains only collinear IR singularity and can be dealt with in the HC region, too. In the $\overline{\rm HC}$ region, the real emission corrections $\hat{\sigma}_{ij}^{\overline{\rm HC}}$, where $ij = q\bar{q}, gg, qg, \bar{q}g$, are finite and can be calculated numerically with the general Monte Carlo method. After summing the virtual and real gluon/(anti) quark radiation corrections, the remained collinear divergence can be canceled by that in the NLO PDFs. Then, the finite total NLO QCD correction to the $pp \to \tilde{t}_1\,\bar{\tilde{t}}_1\,Z^0$ process can be obtained. More details on the calculation of real gluon emission and real light-(anti)quark emission are given in Sec. III B 1 and Sec. III B 2, respectively.

1. Real gluon emission corrections

We denote the partonic processes with real gluon emissions as

$$q(P) + \bar{q}(P) \to \tilde{t}_1(p_3) + \bar{\tilde{t}}_1(p_4) + Z^0(p_5) + g(p_6),$$
$$g(P) + g(P) \to \tilde{t}_1(p_3) + \bar{\tilde{t}}_1(p_4) + Z^0(p_5) + g(p_6). \tag{22}$$

The differential cross section for the partonic processes $q\bar{q} \to \tilde{t}_1\,\bar{\tilde{t}}_1\,Z^0 g$ over the soft gluon region can be expressed as

$$\hat{\sigma}_{\rm soft} = \hat{\sigma}_{\rm LO} \otimes \frac{\alpha_s}{2\pi}\sum_{i,j=1}^{4}(\mathbf{T}_i \cdot \mathbf{T}_j)g_{ij}(p_i, p_j), \tag{23}$$

where T_i are the color operators [22–24], and $g_{ij}(i = 1, 2, 3, j = 2, 3, 4)$ are the soft integrals defined as [12,22]

$$g_{ij}(p_i,p_j)=\frac{(2\pi\mu_r)^{2\epsilon}}{2\pi}\int_{E_6\le\delta_s\sqrt{\hat{s}/2}}\frac{d^{D-1}\mathbf{p_6}}{E_6}\times\left[\frac{2(p_i\cdot p_j)}{(p_i\cdot p_6)(p_j\cdot p_6)}-\frac{p_i^2}{(p_i\cdot p_j)^2}-\frac{p_j^2}{(p_j\cdot p_6)^2}\right]. \tag{24}$$

By using the definitions of color operators, we get the expression of $\sigma^{\rm soft}$ as [22]

$$\hat{\sigma}^{\rm soft}_{g,q\bar{q}}=-\frac{\alpha_s}{2\pi}\left[\frac{1}{6}(g_{12}+g_{34})-\frac{7}{6}(g_{13}+g_{24})-\frac{1}{3}(g_{14}+g_{23})\right]\hat{\sigma}^0_{q\bar{q}}, \tag{25}$$

where

$$\hat{\sigma}^{\rm soft}_{g,gg}=\frac{\alpha_s}{12\pi}\overline{\sum}\left[\left(\frac{256}{3}D_1+16D_3\right)|\mathcal{M}_1^{gg}|^2+\left(\frac{256}{3}D_2+16D_4\right)|\mathcal{M}_2^{gg}|^2+\left(-\frac{32}{3}D_1+16D_3\right)\times 2\mathbf{Re}(\mathcal{M}_1^{gg\dagger}\cdot\mathcal{M}_2^{gg})\right]d\Omega_3, \tag{26}$$

where the summation is taken over the spins and colors of initial and final states, and the bar over the summation represents taking the average over the spins and colors of initial partons, and

$$\mathcal{M}_1^{gg}=\mathcal{M}_t^{gg}+\frac{1}{2}\mathcal{M}_s^{gg},\qquad \mathcal{M}_2^{gg}=\mathcal{M}_u^{gg}-\frac{1}{2}\mathcal{M}_s^{gg}, \tag{27}$$

$\mathcal{M}_s^{gg}$, $\mathcal{M}_t^{gg}$, and $\mathcal{M}_u^{gg}$ are the amplitudes for s-, t-, and u-channel diagrams of the partonic process $gg\to\tilde{t}_1\bar{\tilde{t}}_1 Z^0$ separately, and

$$D_1=9g_{12}+9g_{13}+9g_{24}-g_{34},\quad D_2=9g_{12}+9g_{23}+9g_{14}-g_{34},\quad D_3=6(g_{12}-g_{14}-g_{23}+g_{34}),\quad D_4=6(g_{12}-g_{13}-g_{24}+g_{34}). \tag{28}$$

In the collinear region, the initial-state parton i $(i=q,\bar{q},g)$ is considered to split into a hard parton i' and a collinear gluon g, $i\to i'g$, with $p_{i'}=zp_i$ and $p_6=(1-z)p_i$. The matrix element squared for $q\bar{q}(gg)\to\tilde{t}_1\bar{\tilde{t}}_1 hg$ factorizes into the Born matrix element squared and the Altarelli-Parisi splitting function [25] for $i\to i'g$; i.e.,

$$\overline{\sum}|\mathcal{M}_{\rm HC}(ij\to\tilde{t}_1\bar{\tilde{t}}_1 Z^0 g|^2\simeq(4\pi\alpha_s)\sum_i\overline{\sum}|\mathcal{M}_{\rm LO}(i'j\to\tilde{t}_1\bar{\tilde{t}}_1 Z^0 g)|^2\times\frac{2P_{ii'}(z,\epsilon)}{z(2p_i\cdot p_6)}, \tag{29}$$

where

$$P_{ii'}(z,\epsilon)=P_{ii'}(z)+\epsilon P'_{ii'}(z)\quad(i=q,g),\qquad P_{qq}(z)=C_F\frac{1+z^2}{1-z},\qquad P'_{qq}(z)=-C_F(1-z),$$
$$P_{gg}(z)=2N\left[\frac{z}{1-z}+\frac{1-z}{z}+z(1-z)\right],\qquad P'_{gg}(z)=0, \tag{30}$$

where $N=3$ is the color number $C_F=4/3$.

Using the approximation $p_i-p_6\simeq zp_i$ $(i=1,2)$, the element in the four body collinear phase-space region can be written as [22]

$$d\Phi_4|_{\rm coll}=d\Phi_3\frac{(4\pi)^\epsilon}{16\pi^2\Gamma(1-\epsilon)}zdzd\hat{t}_{i6}[-(1-z)\hat{t}_{i6}]^{-\epsilon}\times\theta\left(\frac{(1-z)}{z}s'\frac{\delta_c}{2}-s_{i6}\right)\quad(i=1,2), \tag{31}$$

where $s'=2p_{i'}\cdot p_j$, $s_{i6}=2q_i\cdot k$, and $\hat{t}_{i6}=(p_i-p_6)^2$. The cross section in the hard-collinear region $d\sigma_{ij}^{\rm HC}$ can be written as [26]

$$\hat{\sigma}_{ij}^{\rm HC}=\left[\frac{\alpha_s}{2\pi}\frac{\Gamma(1-\epsilon)}{\Gamma(1-2\epsilon)}\left(\frac{4\pi\mu^2}{s'}\right)^\epsilon\right]\left(-\frac{1}{\epsilon}\right)\delta_c^{-\epsilon}\times\left\{\int_0^{1-\delta_s}dz\left[\frac{(1-z)^2}{2z}\right]^{-\epsilon}P_{ii'}(z,\epsilon)\times\hat{\sigma}_{\rm LO}(i'j\to\tilde{t}_1\bar{\tilde{t}}_1 Z^0-)+(i\leftrightarrow j)\right\}. \tag{32}$$

2. Real light-(anti)quark emission corrections

The partonic processes with real light-quark emissions are denoted by

$$(q,\bar{q})(P)+g(P)\to\tilde{t}_1(p_3)+\bar{\tilde{t}}_1(p_4)+Z^0(p_5)+(q,\bar{q})(p_6). \tag{33}$$

These partonic processes contain only the initial-state collinear singularities induced by strong interaction. The extraction of the collinear singularities of $\delta\hat{\sigma}^{\rm real}_{q(\bar{q})g}$ is done in the same way as described in Sec. III B 1. Splitting the phase space into HC and $\overline{\rm HC}$ regions by introducing a cutoff δ_c, we can express the cross sections for the partonic processes $q(\bar{q})g\to\tilde{t}_1\bar{\tilde{t}}_1 Z^0 q(\bar{q})$ as

$$\delta\hat{\sigma}^{\rm real}_{q(\bar{q})g} = \hat{\sigma}^{\rm HC}_{q(\bar{q})g} + \hat{\sigma}^{\overline{\rm HC}}_{q(\bar{q})g}. \tag{34}$$

The cross sections in the noncollinear region $\hat{\sigma}^{\overline{\rm HC}}_{q(\bar{q})g}$ are finite and can be evaluated in four dimensions by using the Monte Carlo method. The cross sections in the collinear region for the $pp \to q(\bar{q})g \to \tilde{t}_1 \bar{\tilde{t}}_1 Z^0 q(\bar{q})$ processes can be written as

$$\begin{aligned}\hat{\sigma}^{\rm HC}_{qg} = &\left[\frac{\alpha_s}{2\pi}\frac{\Gamma(1-\epsilon)}{\Gamma(1-2\epsilon)}\left(\frac{4\pi\mu^2}{s'}\right)^{\epsilon}\right] \\ &\times \left(-\frac{1}{\epsilon}\right)\delta_c^{-\epsilon}\left\{\int_0^{1-\delta_s} dz \left[\frac{(1-z)^2}{2z}\right]^{-\epsilon}\right. \\ &\left.\times P_{qg}(z,\epsilon)\hat{\sigma}^{\rm LO}_{gg} + P_{gq}(z,\epsilon)\hat{\sigma}^{\rm LO}_{qq}\right\},\end{aligned} \tag{35}$$

where the splitting functions $P_{qg(gq)}(z,\epsilon)$ can be written explicitly as [27]

$$\begin{aligned}P_{qg,gq}(z,\epsilon) &= P_{qg,gq}(z) + \epsilon P'_{qg,gq}(z), \\ P_{qg}(z) &= \frac{1}{2}[z^2 + (1-z)^2], \\ P'_{qg}(z) &= -z(1-z), \\ P_{gq}(z) &= C_F\frac{1+(1-z)^2}{z}, \\ P'_{gq}(z) &= -C_F z.\end{aligned} \tag{36}$$

C. The total cross section for $pp \to \tilde{t}_1 \bar{\tilde{t}}_1 Z^0$ at NLO SUSY-QCD correction

The total hadronic cross section for $pp \to \tilde{t}_1 \bar{\tilde{t}}_1 Z^0$ is given by

$$\begin{aligned}\sigma^{\rm NLO} = &\sum_{ij=q\bar{q},gg}\frac{1}{1+\delta_{ij}}\int dx_1 dx_2 \\ &\times [\mathcal{F}^P_i(x_1,\mu)\mathcal{F}^P_j(x_2,\mu)\hat{\sigma}^{\rm NLO}_{ij}(x_1,x_2,\mu) + (1 \leftrightarrow 2)],\end{aligned} \tag{37}$$

where $\mathcal{F}^P_i$ are the NLO PDFs for parton i in a proton, defined at a generic factorization scale $\mu_f = \mu$, and $\hat{\sigma}^{\rm NLO}_{ij}$ is the $\mathcal{O}(\alpha_s^3)$ parton-level total cross section for incoming partons i and j and renormalized at $\mu_r = \mu$. The NLO parton-level total cross section $\hat{\sigma}^{\rm NLO}_{ij}(x_1,x_2,\mu)$ can be written as

$$\hat{\sigma}^{\rm NLO}_{ij}(x_1,x_2,\mu) = \hat{\sigma}^{\rm LO}_{ij}(x_1,x_2,\mu) + \delta\hat{\sigma}^{\rm NLO}_{ij}(x_1,x_2,\mu), \tag{38}$$

where $\hat{\sigma}^{\rm LO}_{ij}(x_1,x_2,\mu)$ is the $\mathcal{O}(\alpha_s^2)$ Born cross section, and $\delta\hat{\sigma}^{\rm NLO}_{ij}(x_1,x_2,\mu)$ consists of the $\mathcal{O}(\alpha_s)$ corrections to the Born cross sections for $gg \to \tilde{t}_1 \bar{\tilde{t}}_1 Z^0$, $q\bar{q} \to \tilde{t}_1 \bar{\tilde{t}}_1 Z^0$, and $(q,\bar{q})g \to \tilde{t}_1 \bar{\tilde{t}}_1 Z^0(q,\bar{q})$ processes, including the effects of mass factorization.

The remaining initial-state IR singularities of $\delta\hat{\sigma}^{\rm NLO}_{ij}$ can be canceled by decomposing the collinear counterterms of the PDF $\mathcal{F}^p_i(x,\mu)$ into two parts: the collinear gluon emission part $\mathcal{F}^P_g(x,\mu)$ and the collinear light-quark emission part $\mathcal{F}^P_q(x,\mu)$ as follows:

$$\mathcal{F}^p_i(x,\mu) = \mathcal{F}^P_g(x,\mu) + \mathcal{F}^P_q(x,\mu). \tag{39}$$

Using the $\overline{\rm MS}$ scheme, the scale-dependent NLO quark distribution functions are given in terms of $\mathcal{F}^P_q(x)$ and the QCD NLO parton distribution function counterterms [26] as follows:

$$\begin{aligned}\mathcal{F}^P_q(x,\mu) = &\mathcal{F}^P_q(x)\left[1 - \frac{\alpha_s}{2\pi}\frac{\Gamma(1-\epsilon)}{\Gamma(1-2\epsilon)}(4\pi)^{\epsilon}\left(\frac{1}{\epsilon}\right)\right. \\ &\left.\times C_F\left(2\ln(\delta_s) + \frac{3}{2}\right)\right] + \left[\frac{\alpha_s}{2\pi}\frac{\Gamma(1-\epsilon)}{\Gamma(1-2\epsilon)}(4\pi)^{\epsilon}\right] \\ &\times \int_x^{1-\delta_s}\frac{dz}{z}\left(-\frac{1}{\epsilon}\right)P_{qq}(z)\mathcal{F}^P_q\left(\frac{x}{z}\right),\end{aligned} \tag{40}$$

$$\begin{aligned}\mathcal{F}^P_g(x,\mu) = &\mathcal{F}^P_g(x)\left[1 - \frac{\alpha_s}{2\pi}\frac{\Gamma(1-\epsilon)}{\Gamma(1-2\epsilon)}(4\pi)^{\epsilon}\left(\frac{1}{\epsilon}\right)\right. \\ &\left.\times N\left(2\ln(\delta_s) + \frac{11}{6} - \frac{1}{3}\frac{n_{lf}}{N}\right)\right] \\ &+ \left[\frac{\alpha_s}{2\pi}\frac{\Gamma(1-\epsilon)}{\Gamma(1-2\epsilon)}(4\pi)^{\epsilon}\right] \\ &\times \int_x^{1-\delta_s}\frac{dz}{z}\left(-\frac{1}{\epsilon}\right)P_{gg}(z)\mathcal{F}^P_g\left(\frac{x}{z}\right).\end{aligned} \tag{41}$$

By combining the contributions of the PDF counterterms with the hard-collinear contributions of the $q\bar{q} \to \tilde{t}_1 \bar{\tilde{t}}_1 Z^0 g$, $gg \to \tilde{t}_1 \bar{\tilde{t}}_1 Z^0 g$, and $q(\bar{q})g \to \tilde{t}_1 \bar{\tilde{t}}_1 Z^0 q(\bar{q})$ subprocesses, we get the expression for the remaining collinear contributions σ^C to the process $pp \to \tilde{t}_1 \bar{\tilde{t}}_1 Z^0$ in $\mathcal{O}(\alpha_s)$ order as

$$\begin{aligned}\sigma^C = &\left[\frac{\alpha_s}{2\pi}\frac{\Gamma(1-\epsilon)}{\Gamma(1-2\epsilon)}\left(\frac{4\pi\mu^2}{\hat{s}}\right)^{\epsilon}\right]\sum_{ij=u\bar{u},d\bar{d}}^{gg}\frac{1}{1+\delta_{ij}} \\ &\times \int_0^1 dx_1 \int_0^1 dx_2 \times \left\{\left[\tilde{\mathcal{F}}^P_i(x_1,\mu)\mathcal{F}^P_j(x_2,\mu)\right.\right. \\ &+ \mathcal{F}^P_i(x_1,\mu)\tilde{\mathcal{F}}^P_j(x_2,\mu) \\ &\left.+ \sum_{\alpha=i,j}\left(\frac{A_1^{sc}(\alpha \to \alpha g)}{\epsilon} + A_0^{sc}(\alpha \to \alpha g)\right)\right]\hat{\sigma}^{\rm LO}_{ij} \\ &\left.+ (i \leftrightarrow j)\right\},\end{aligned} \tag{42}$$

where

$$A_1^{sc}(q \to qg) = C_F(2\ln\delta_s + 3/2),$$
$$A_1^{sc}(g \to gg) = 2N\ln\delta_s + (11N - 2n_{lf})/6,$$
$$A_0^{sc} = A_1^{sc}\ln\left(\frac{\hat{s}}{\mu_f^2}\right),$$
$$\tilde{\mathcal{F}}_\alpha^P(x,\mu) = \sum_{\alpha'}\int_x^{1-\delta_s\delta_{\alpha\alpha'}}\frac{dy}{y}\mathcal{F}_{\alpha'}^P(x/y,\mu)\tilde{P}_{\alpha\alpha'}(y),$$
$$\tilde{P}_{\alpha\alpha'}(y) = P_{\alpha\alpha'}(y)\ln\left(\delta_c\frac{1-y}{y}\frac{\hat{s}}{\mu_f^2}\right) - P'_{\alpha\alpha'}(y), \tag{43}$$

where $P_{\alpha\alpha'}$ and $P'_{\alpha\alpha'}$ can be found in Ref. [26].

The normalized distribution function counterterms exactly cancel the remaining IR singularities $\hat{\sigma}_{ij}^{\rm virt} + \hat{\sigma}_{ij}^{\rm soft}$ and $\hat{\sigma}^C$. The complete cross section for $pp \to \tilde{t}_1\bar{\tilde{t}}_1 Z^0$ in the $\overline{\rm MS}$ factorization scheme can be written as follows:

$$\sigma^{\rm NLO} = \int \sigma^C + \sum_{ij=u\bar{u},d\bar{d}}^{gg}\frac{1}{1+\delta_{ij}}\int_0^1 dx_1\int_0^1 dx_2\int[(\hat{\sigma}_{ij}^{\rm virt} + \hat{\sigma}_{g,ij}^{\rm soft})\mathcal{F}_i^P(x_1,\mu)\mathcal{F}_j^P(x_2,\mu) + (i \leftrightarrow j)]$$
$$+ \sum_{ij=u\bar{u},d\bar{d}}^{gg}\frac{1}{1+\delta_{ij}}\int_0^1 dx_1\int_0^1 dx_2[\mathcal{F}_i^P(x_1,\mu)\mathcal{F}_j^P(x_2,\mu)\hat{\sigma}_{g,ij}^{\overline{\rm HC}} + (i \leftrightarrow j)]$$
$$+ \sum_{q=u,d}^{\bar{u},\bar{d}}\int_0^1 dx_1\int_0^1 dx_2[\mathcal{F}_q^{P_1}(x_1,\mu)\mathcal{F}_g^P(x_2,\mu)\hat{\sigma}_{qg}^{\overline{\rm HC}} + (q \leftrightarrow g)], \tag{44}$$

with the hard-noncollinear partonic cross section given by

$$\hat{\sigma}_{ij}^{\overline{\rm HC}} = \int_{\overline{\rm HC}}\overline{\sum}|M(ij \to \tilde{t}_1\bar{\tilde{t}}_1 Z^0 + g(q,\bar{q}))|^2 d\Phi_4. \tag{45}$$

IV. RESULTS AND DISCUSSIONS

In this section, we present numerical results of the NLO SUSY-QCD corrections to the process $pp \to \tilde{t}_1\bar{\tilde{t}}_1 Z^0$ in the MSSM. We consider the benchmark point $SPS1a$ scenario, which is proposed in the *SPA* Convention and Project [28–30], as a numerical demonstration. The relevant masses of SUSY particles and parameters at the $SPS1a$ point required in our numerical calculations are listed in Table I. We have generated the spectrum of masses, couplings, and mixings relative to squarks by running the mSUGRA program contained in the package ISAJET [31], version 7.69. The values of the Z^0 and top masses we used are 91.1876 and 175 GeV, respectively.

TABLE I. Relevant SUSY parameters obtained by using ISAJET 7.82 with the input parameters at the reference point $SPS1a$.

Particle	Mass (GeV)	Particle	Mass (GeV)
$\tilde{t}_1$	377.39	$\tilde{u}_R$	545.95
$\tilde{t}_2$	571.62	$\tilde{u}_L$	562.33
$\tilde{g}_2$	604.00	$\tilde{d}_R$	545.67
		$\tilde{d}_L$	567.83
SUSY parameter		SUSY parameter	
$M_0 = -A_0$	100.00 GeV	sign(μ)	+
$\tan\beta$	10.0	$M_{1/2}$	250.00

The numerical analyses of the hadronic cross sections have been performed for the CERN LHC with pp centers of mass of $\sqrt{s} = 7$ and 14 TeV. The hadronic cross sections are obtained

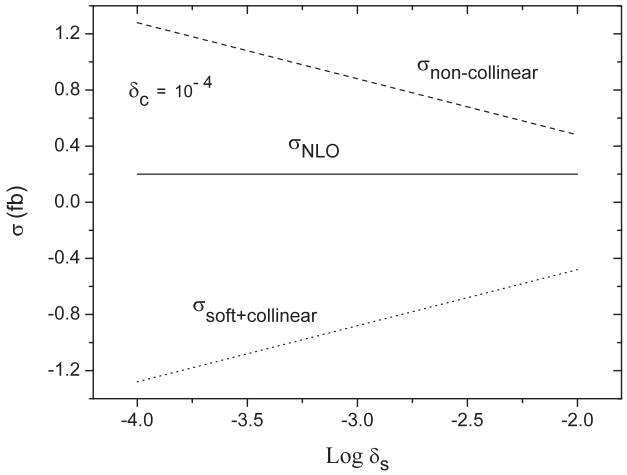

FIG. 4. Dependence of $\sigma^{\rm NLO}$ ($pp \to \tilde{t}_1\bar{\tilde{t}}_1 Z^0$) on the soft cutoff δ_s of the two-cutoff method, at 7 TeV, for $\mu = m_{\tilde{t}_1} + \frac{M_{Z^0}}{2}$ and $\delta_c = 10^{-4}$.

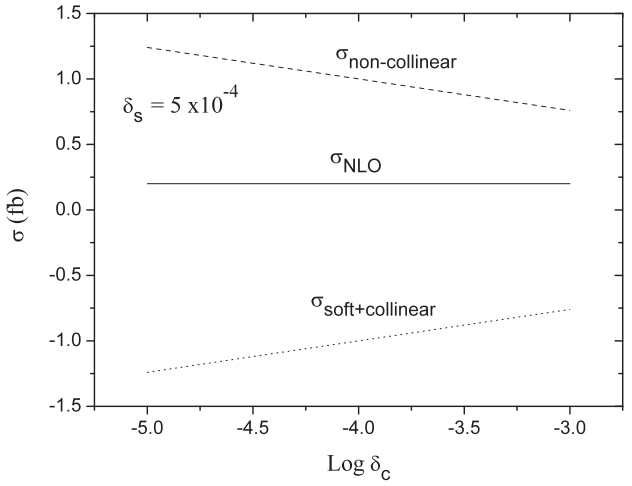

FIG. 5. Dependence of σ^{NLO} $(pp \to \tilde{t}_1 \bar{\tilde{t}}_1 Z^0)$ on the collinear cutoff δ_c of the two-cutoff method, at 7 TeV, for $\mu = m_{\tilde{t}_1} + \frac{M_{Z^0}}{2}$ and $\delta_s = 5 \times 10^{-4}$.

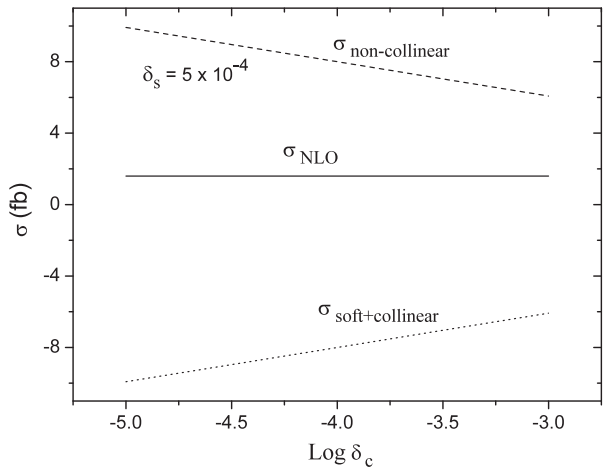

FIG. 7. Dependence of σ^{NLO} $(pp \to \tilde{t}_1 \bar{\tilde{t}}_1 Z^0)$ on the collinear cutoff δ_c of the two-cutoff method, at 14 TeV, for $\mu = m_{\tilde{t}_1} + \frac{M_{Z^0}}{2}$ and $\delta_s = 5 \times 10^{-4}$.

by convoluting the partonic cross sections with the parton distribution functions of the initial-state hadrons. Our numerical results are obtained using CTEQ6L1 PDFs [32] with a one-loop running α_s in the LO calculation and CTEQ6M PDFs [33,34] with a two-loop α_s in the NLO calculation. By default, we set the renormalization and factorization scales to the common scale μ and we define $\mu_0 = m_{\tilde{t}_1} + m_Z^0/2$. The number of active flavors is $N_f = 2$, and the QCD parameters are $\Lambda_5^{\mathrm{LO}} = 166$ MeV and $\Lambda_5^{\overline{\mathrm{MS}}} = 227$ MeV for the LO and NLO calculations, respectively [33].

In Figs. 4 and 5, we consider the two-cutoff phase-space slicing method at the 7 TeV LHC and study the independence of σ^{NLO} on δ_s and δ_c separately, by varying only one of the two cutoffs while the other is kept fixed. In these plots, we show the overall cutoff dependence cancellation between $\sigma_{\mathrm{soft}} + \sigma_{\mathrm{hard/coll}}$ and $\sigma_{\mathrm{noncollinear}}$. Both Figs. 4 and 5 show a clear plateau over a wide range of δ_s and δ_c, and the NLO cross section is proven to be cutoff independent. Similar plots are presented in Figs. 6 and 7 at the 14 TeV LHC.

The LO and NLO cross sections for $\tilde{t}_1 \bar{\tilde{t}}_1 Z^0$ production at the LHC as the functions of the renormalization and factorization scale μ are plotted in Figs. 8 and 9 corresponding to $\sqrt{s} = 7$ and 14 TeV, respectively. As shown in Figs. 8 and 9, the curve for the NLO cross section is much less sensitive to μ than the one for the LO cross section, which indicates that the NLO SUSY-QCD correction has obviously reduced the uncertainty of the cross section on the introduced parameter μ in the plotted range of μ/μ_0. Indeed, as can be seen in Figs. 8 and 9, the scale

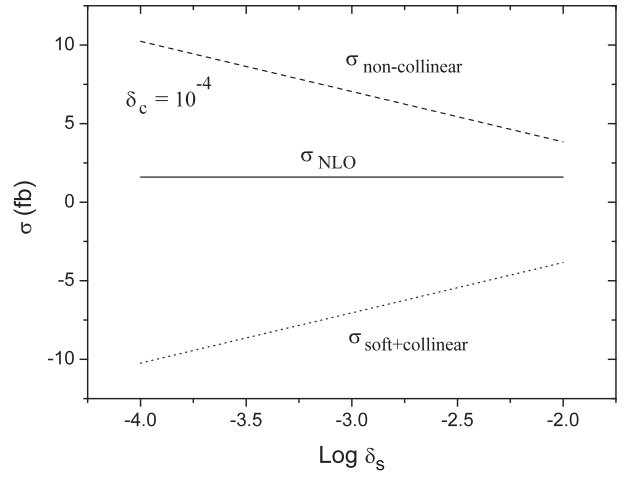

FIG. 6. Dependence of σ^{NLO} $(pp \to \tilde{t}_1 \bar{\tilde{t}}_1 Z^0)$ on the soft cutoff δ_s of the two-cutoff method, at 14 TeV, for $\mu = m_{\tilde{t}_1} + \frac{M_{Z^0}}{2}$ and $\delta_c = 10^{-4}$.

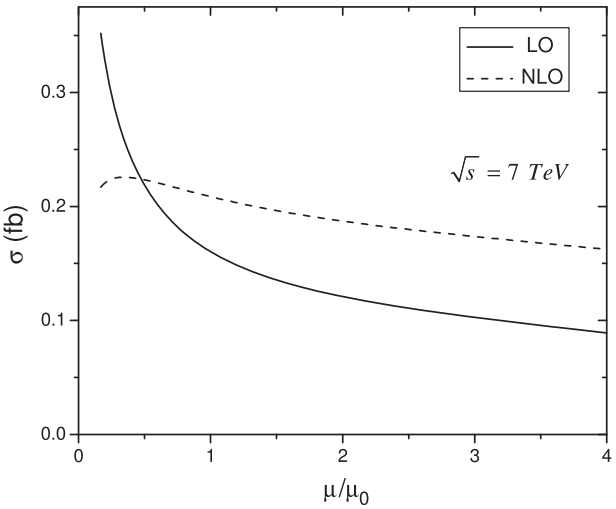

FIG. 8. Scale dependence of the LO and NLO cross section at the 7 TeV LHC.

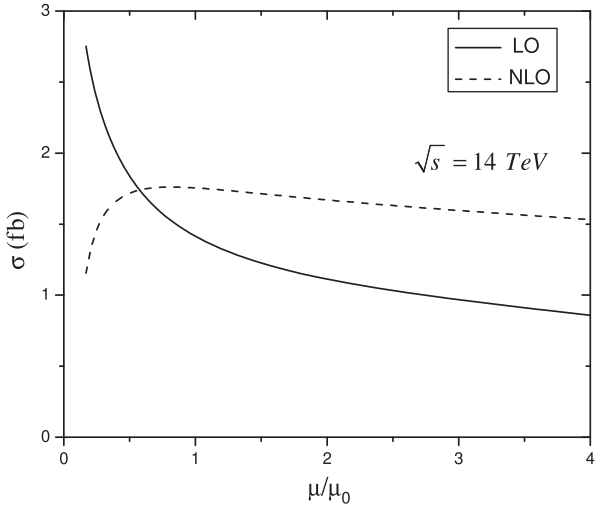

FIG. 9. Scale dependence of the LO and NLO cross section at the 14 TeV LHC.

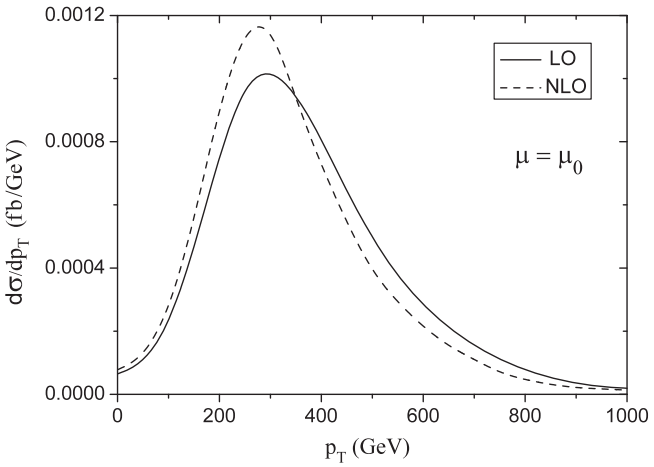

FIG. 10. LO and NLO transverse-momentum distributions for stop at the 7 TeV LHC for $\mu = \mu_0$.

dependence of the LO and NLO curves is similar for both 7 and 14 TeV. The LO cross section has 65% and 54% uncertainties, due to scale dependence, for both 7 and 14 TeV, respectively. These uncertainties are reduced at NLO to about 27% for the 7 TeV and to about 14% for the 14 TeV cross sections. The uncertainties have been

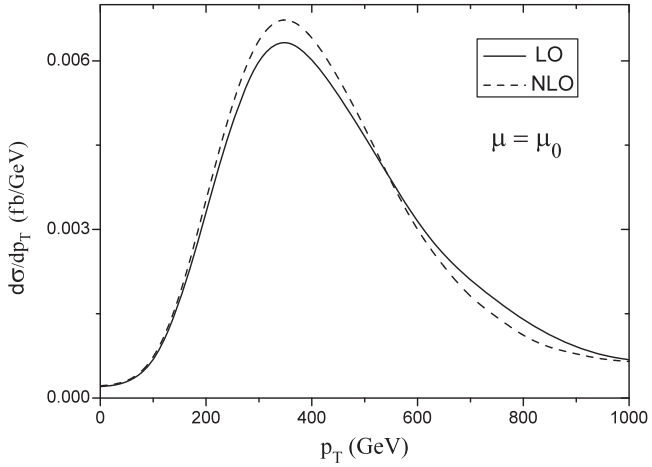

FIG. 11. LO and NLO transverse-momentum distributions for stop at the 14 TeV LHC for $\mu = \mu_0$.

estimated as the positive/negative deviation with respect to the midpoint of the bands. The bands are obtained by varying μ between μ_0 and $4\mu_0$.

The LO and NLO distributions of the transverse momenta of the final stop quark are depicted in Figs. 10 and 11 at 7 and 14 TeV, respectively. Figures 10 and 11 demonstrate that the NLO QCD corrections enhance significantly the distributions of $p_T^{(\tilde{t}_1)}$.

V. CONCLUSIONS

In this paper, we calculate the NLO SUSY-QCD corrections to the process $pp \to \tilde{t}_1 \bar{\tilde{t}}_1 Z^0$ in the MSSM at the 7 and 14 TeV LHC. As a numerical demonstration, we present and discuss the NLO SUSY-QCD corrections around the $SPS1a$ benchmark point. We investigate the dependence of the LO and NLO SUSY-QCD corrected cross sections on the factorization/renormalization energy scale. We demonstrate that the uncertainty of the LO cross section caused by the introduced energy scale is significantly improved by including the NLO SUSY-QCD corrections. We present the transverse-momentum distributions of the stop quark, at the 7 and 14 TeV LHC, and provide the NLO SUSY-QCD corrected distributions. We find that the NLO SUSY-QCD contributions remarkably affect the distributions.

[1] S. L. Glashow, Nucl. Phys. **22**, 579 (1961); S. Weinberg, Phys. Rev. Lett. **19**, 1264 (1967); A. Salam, in *Proceedings of the 8th Nobel Symposium, Stockholm, 1968*, edited by N. Svartholm (Almqvist & Wiskells, Stockholm, 1968); S. L. Glashow, J. Iliopoulos, and L. Maiani, Phys. Rev. D **2**, 1285 (1970); H. Fritzsch, M. Gell-Mann, and H. Leutwyler, Phys. Lett. **47B**, 365 (1973); E. S. Abers and B. W. Lee, Phys. Rep. **9**, 1 (1973); S. F. Novaes, arXiv:hep-ph/0001283.

[2] H. P. Nilles, Phys. Rep. **110**, 1 (1984); H. E. Haber and G. L. Kane, Phys. Rep. **117**, 75 (1985).

[3] J. F. Gunion and H. E. Haber, Nucl. Phys. **B272**, 1 (1986).
[4] A. H. Chamseddine, R. Arnowitt, and P. Nath, Phys. Rev. Lett. **49**, 970 (1982).
[5] L. Ibanez and G. Ross, Phys. Lett. **110B**, 215 (1982); L. Ibanez, Phys. Lett. **118B**, 73 (1982); J. Ellis, D. Nanopoulos, and K. Tamvakis, Phys. Lett. **121B**, 123 (1983).
[6] H. A. El-Kolaly and S. M. Seif, Phys. Rev. D **83**, 074002 (2011).
[7] H. E. Haber and G. L. Kane, Phys. Rep. **117**, 75 (1985).
[8] T. Hahn, Comput. Phys. Commun. **140**, 418 (2001).
[9] J. A. Vermaseren, arXiv:math-ph/0010025.
[10] G.'t Hooft and M. Veltman, Nucl. Phys. **B153**, 365 (1979); G. Passarino and M. Veltman, Nucl. Phys. **B160**, 151 (1979).
[11] G. J. van Oldenborgh and J. A. Vermaseren, Z. Phys. C **46**, 425 (1990).
[12] L. Reina, S. Dawson, and D. Wackeroth, Phys. Rev. D **65**, 053017 (2002).
[13] Z. Bern, L. Dixon, and D. A. Kosower, Phys. Lett. B **302**, 299 (1993).
[14] Z. Bern, L. J. Dixon, and D. A. Kosower, Nucl. Phys. **B412**, 751 (1994).
[15] A. Denner, Fortschr. Phys. **41**, 307 (1993).
[16] W. Hollik and H. Rzehak, Eur. Phys. J. C **32**, 127 (2003).
[17] S. Heinemeyer, W. Hollik, H. Rzehak, and G. Weiglein, Eur. Phys. J. C **39**, 465 (2005).
[18] W. Hollik and E. Mirabella, J. High Energy Phys. 12 (2008) 087.
[19] B. W. Harris and J. F. Owens, Phys. Rev. D **65**, 094032 (2002).
[20] W. T. Giele and E. W. N. Glover, Phys. Rev. D **46**, 1980 (1992); W. T. Giele, E. W. Glover, and D. A. Kosower, Nucl. Phys. **B403**, 633 (1993).
[21] S. Keller and E. Laenen, Phys. Rev. D **59**, 114004 (1999).
[22] W. Beenakker, S. Dittmaier, M. Kramer, B. Plumper, M. Spira, and P. M. Zerwas, Phys. Rev. Lett. **87**, 201805 (2001); Nucl. Phys. **B653**, 151 (2003).
[23] S. Catani and M. H. Seymour, Phys. Lett. B **378**, 287 (1996); Nucl. Phys. **B485**, 291 (1997).
[24] S. Catani, S. Dittmaier, M. H. Seymour, and Z. Trócsányi, Nucl. Phys. **B627**, 189 (2002).
[25] G. Altarelli and G. Parisi, Nucl. Phys. **B126**, 298 (1977).
[26] B. W. Harris and J. F. Owens, Phys. Rev. D **65**, 094032 (2002).
[27] G. Altarelli and G. Parisi, Nucl. Phys. **B126**, 298 (1977).
[28] J. A. Aguilar-Saavedra *et al.*, Eur. Phys. J. C **46**, 43 (2006).
[29] B. C. Allanach *et al.*, Eur. Phys. J. C **25**, 113 (2002).
[30] N. Ghodbane and H.-U. Martyn, arXiv:hep-ph/0201233.
[31] http://www.nhn.ou.edu/~isajet/; H. Baer *et al.*, arXiv:hep-ph/0312045.
[32] J. Pumplin, D. Robert Stump, J. Huston, H.-L. Lai, P. Nadolsky, and W.-K. Tung, J. High Energy Phys. 07 (2002) 012; D. Stump, J. Huston, J. Pumplin, W.-K. Tung, H.-L. Lai, S. Kuhlmann, and J. Francis Owens, J. High Energy Phys. 10 (2003) 046.
[33] C. Amsler *et al.*, Phys. Lett. B **667**, 1 (2008).
[34] H. L. Lai, J. Huston, S. Kuhlmann, J. Morfin, F. Olness, J. F. Owens, J. Pumplin, and W. K. Tung, Eur. Phys. J. C **12**, 375 (2000).